Revision 1

Factors controlling the crystal morphology and chemistry of garnet in skarn deposits: a case study from the Cuihongshan polymetallic deposit, Lesser Xing'an Range, NE China

Xianghui Fei[a], Zhaochong Zhang[a*], Zhiguo Cheng[a], M. Santosh[a,b]

[a]State Key Laboratory of Geological Processes and Mineral Resources, China University of Geosciences, Beijing 100083, China

[b]Department of Earth Sciences, University of Adelaide, SA 5005, Australia

Corresponding author: E-mail: zczhang@cugb.edu.cn

Abstract

The grossular-andradite solid solutions in garnet from skarn deposits in relation to hydrothermal processes and physicochemical conditions of ore formation remain controversial. Here we investigate garnet occurring in association with calcic and magnesian skarn rocks in the Cuihongshan polymetallic skarn deposit of NE China. The calcic skarn rocks contain three types of garnets. 1) Prograde type I Al-rich anisotropic garnets display polysynthetic twinning and a compositional range of $Grs_{18-80}Adr_{10-75}$. This type of garnet shows markedly low rare earth element (REE) contents (3.27-78.26 ppm), and are strongly depleted in light rare earth elements (LREE, 0.57-44.65 ppm) relative to heavy rare earth elements (HREE, 2.31-59.19 ppm). They also display significantly negative Eu anomaly (Eu/Eu* of 0.03-0.90). 2)

Fe-rich retrograde type II garnets are anisotropic with oscillatory zoning and own wide compositional variations ($Grs_{1-47}Adr_{30-95}$) with flat REE (13.73-377.08 ppm) patterns. 3) Fe-rich retrograde type III isotropic garnets display oscillatory zoning and morphological transition from planar dodecahedral {110} crystal faces to {211} crystal faces in the margin. Types III garnets exhibit relatively narrow compositional variations of $Grs_{0.1-12}Adr_{85-97}$ with LREE-enrichment (0.80-51.87 ppm), flat HREE patterns (0.15-2.46 ppm) and strong positive Eu anomalies (Eu/Eu* of 0.93-27.07 with almost >1). The magnesian skarn rocks contain euhedral isotropic type IV Mn-rich garnet veins with a composition of $Grs_{10-23}Sps_{48-62}Alm_{14-29}$. All calcic garnets contain considerable Sn and W contents. Type II garnet containing intermediate compositions of andradite and grossular shows the highest Sn contents (64.36-2778.92 ppm) albeit the lowest W range (1.11-468.44 ppm). Birefringence of garnet is probably caused by strain from lattice mismatch in twinning boundary or ion substitution near intermediate compositions of grossular-andradite. The fine-scale, sharp and straight garnet zones are probably caused by self-organization, but the compositional variations of zones from core to rim are probably caused by external factors. The zoning is likely driven by external factors such as composition of the hydrothermal fluid. Grossular-andradite solid solution exhibits an asymmetric Margules model. REE concentrations are probably influenced by the relative proportion and temperature of the system. Moreover, the LREE-HREE fractionation of garnet can be attributed to relative compositions of grossular-andradite system. The W and Sn concentrations in garnet can be used as indicators for the exploration of

W-Sn skarn deposits.

Keywords:

Garnet; Birefringence; Substitution of REE; Skarn; Cuihongshan polymetallic deposit

1 Introduction

Garnet is a major mineral in skarn rocks, and has been divided into pyralspite (pyrope, almandine, spessartine) and ugrandite (uvarovite, grossular, andradite) groups (Grew et al. 2010), among which the grossular-andradite solid solutions are the most common types. Their formation is controlled by the nature of skarn deposit types, and related hydrothermal processes as well physicochemical conditions (e.g., Einaudi and Burt 1982; Orhan 2017; Xie et al. 2019).

Meinert et al. (2005) proposed ternary plots to evaluate the relationship between different skarn types and garnet compositions. Recent studies on skarn deposits suggest that garnet compositions might display complex relationship depending on the skarn types, and that the composition is controlled by multiple factors, offering a challenge to characterize the types and composition of garnet in diverse skarn associations (Ciobanu and Cook 2004; Baghban et al. 2016).

The Cuihongshan polymetallic skarn deposit located in the Lesser Xing’an Range in NE China contains abundant garnet grains occurring in association with calcic and magnesian skarn rocks and related to multiple ore-forming stages. This occurrence offers a rare opportunity to explore the factors controlling garnet formation in polymetallic skarn systems. In this paper, we present a detailed study of garnet mineralogy including texture as well as the major and trace element compositions of garnets from different associations and stages, with a view to constrain the factors controlling garnet formation. Our data provide important insights into garnet formation in skarn deposits with complex evolutionary history.

2 Geological Setting

The Cuihongshan polymetallic deposit is located in the central part of the Lesser Xing'an Range in the eastern part of the Central Asian Orogenic Belt (CAOB) (Fig. 1). The basement of the Lesser Xing'an Range is composed of the Proterozoic Dongfengshan Complex that comprises mica schist, mica-quartz schist, graphite schist, andalusite schist and marble with fluorine-bearing banded iron formations (BIF). The basement is overlain by Cambrian-Ordovician carbonates, terrigenous clastic rocks, volcanic rocks and sandstones. The dominant granitoids in the Lesser Xing'an Range are composed of late Proterozoic, Paleozoic and Mesozoic intrusions. Several mafic and ultramafic intrusions have also been recognized in the region (Yu et al. 2012).

The "L-shaped" mining area of the Cuihongshan polymetallic deposit occupies three sections including the Cuihongshan section in the north and the Cuigang and Cuinan sections in the south. The Cuihongshan deposit is composed of 106 orebodies among which 10 are of large-scale. Underground mining is currently going on in the Cuihongshan section which occupies an area of 2.4 km^2 and contains six large-scale orebodies including porphyry-type molybdenite orebodies hosted in Mesozoic porphyritic granite, together with orebodies of skarn scheelite-molybdenite, skarn magnetite, skarn magnetite-sphalerite and skarn chalcopyrite-galena-sphalerite. The deposit hosts an estimated ore resource of 39.4 Mt iron-ore with 30-58% Fe, 0.09 Mt Mo with a grade of 0.03-0.13% Mo, 0.12 Mt WO_3 with a grade of 0.60-0.21% WO_3, 0.19 Mt Pb with average Pb grade of 1.65% and 0.51 Mt Zn with average Zn grade of 3.15% (Fei et al. 2018, and reference therein).

Three major lithological units were identified in the ore district, including rocks belonging to the Proterozoic Dongfengshan Complex as the basement, sedimentary units of the Early Cambrian Qianshan Formation, and the Early Paleozoic and Early Mesozoic granitic intrusions representing two major magmatic events (Fig. 2). The Dongfengshan Complex experienced greenschist to amphibolite facies metamorphism, and the rocks are overlain by the Cambrian Qianshan Formation. The Qianshan Formation is the major wall rocks for skarn mineralization and is composed of recrystallized dolomitic limestone, calcic limestone, dolomite, hornfelsic sandstone, siltstone and slate. Most of the intrusions are concealed below the surface. The Paleozoic intrusions are distributed mainly in the central part of the ore district and include biotite syenogranite and biotite porphyritic granite. There is a gradual transition from the biotite syenogranite outwards to the biotite porphyritic granite. The Mesozoic granitic intrusions contain porphyritic quartz monzonite, monzogranite and porphyritic granite. The porphyritic quartz monzonite is located far from the deposit without any direct contact with the orebodies whereas the monzogranite is exposed in the western, southeastern and northeastern parts of the area, mainly as stocks. The porphyritic granite is located close to the orebodies in the western part of the mining area (Fig. 2). The porphyry Mo mineralization occurs within the Mesozoic porphyritic granite. The reddish Mo ores occur as 5-15% vol. percent of irregular disseminations or aggregates. The W-Mo ores are disseminated in the calcic skarn rocks occurring adjacent to the Mesozoic porphyritic granite. Magnetite orebodies are distributed in the calcic skarn rocks next to the W-Mo skarn orebodies. A small number of magnetite-sphalerite skarn orebodies are located next to the magnetite orebodies in the magnesian skarn rocks. Moreover, sporadic galena-sphalerite ores are also found adjacent the magnetite-sphalerite orebody in the magnesian skarn rocks (Fig. 2). Most of the skarn rocks in this deposit are located in the contact zone between the Mesozoic porphyritic granite and Qianshan Formation with recent studies correlating the polymetallic mineralization to the Mesozoic porphyritic granite (Fei et al. 2018).

Several faults and folds are developed in the district. The Cuihongshan deposit is distributed along an NWN structural zone formed by the NEN and WNW conjugate fractures. An NEN-trending composite fold extends throughout the ore district (Hu et al. 2014).

In general, the wall-rock alteration is pervasive, but the original magmatic texture and the shape of most minerals are preserved, except for the Mesozoic porphyritic granite close to the orebodies which is almost replaced by the skarn minerals (Fei et al. 2018).

3. Skarn

The orebodies display complex shapes in the skarn rocks and the distribution of skarn rocks is controlled by the contact zone between ore-related Mesozoic granite and limestone, regional NWN structural zone and the structurally weak zones among the Paleozoic granite, ore-related Mesozoic granite and sedimentary rocks (Fig. 2). Calcic and magnesian skarn rocks occur in the eastern and western parts of the Cuihongshan mine respectively, and their occurrence is controlled by the wall rock composition (Fig. 2). The endoskarn is much larger in size than the exoskarn (Fei et al. 2018). Garnet is ubiquitous in the mining area. The endoskarn region contains most of the prograde stage minerals and part of the retrograde minerals in the calcic skarn zones. The exoskarn region is characterized by most of the retrograde stage minerals and sulfide stage minerals in the calcic skarn rocks and almost all of the magnesian skarn rocks.

3.1 Calcic Skarn

The calcic skarn occurs at the contact zone between granitic rocks and limestone as well as its recrystallized domains (Fig. 2). The calcic skarn contains scheelite-molybdenite, magnetite and sphalerite skarn orebodies. Based on the field observation, the three types of garnet are identified in the calcic skarn rocks within different alteration zones. The later formed alteration zone has replaced the early-formed zone (Fig. 2). Prograde stage has produced type I garnet (Fig. 3a-e), pyroxene (Fig.3c), plagioclase, fluorine and zircon together with scheelite and some cassiterite. Type I garnet is cut by diopside (Fig.3c). The retrograde stage has produced two types of garnet (II and III, Fig. 3f-m), and the assemblage includes vesuvianite, actinolite, tremolite, zoisite, epidote, fluorite and apatite together with magnetite and most of the cassiterite. Type III garnet cuts the early formed garnet, diopside and magnetite (Fig. 3j-l). The sulfide stage has produced molybdenite, sphalerite, pyrite, bornite and chalcopyrite together with quartz and fluorite (Fei et al. 2018). In general, some of the early-fromed garnet grains in the calcic skarn rocks always occur in the W-Mo orebodies-related endoskarn region characterized by garnet (I and II) + pyroxene + vesuvianite + actinolite + zoisite + fluorite + episode + apatite together with scheelite, cassiterite and molybdenite. This zone occurs adjacent to the Mesozoic granite. The later-formed garnet grains are more commonly seen in the exoskarn region with magnetite orebodies carries garnet (II, III) + fluorite + diopside + tremolite + actinolite + calcite + chlorite together with magnetite, cassiterite, sphalerite and pyrite. The early formed garnet is cut by the later formed garnet in the alteration zone.

3.2 Magnesian Skarn

The magnesian skarn rocks and associated magnetite-, sphalerite-, chalcopyrite-, and lead- skarn orebodies are developed at the contact zone between granitic rocks and dolomite and dolomitic limestone (Fig. 2). The magnesian skarn rocks include pyroxene, minor type IV garnet (Fig. 3n-p), humite, tremolite, phlogopite, serpentine and apatite. Magnetite and cassiterite are the major ore minerals in the retrograde stage. Pyrite, chalcopyrite, sphalerite, bornite, galena and arsenopyrite belong to the sulfide stage, and some specularite formed in the supergene stage (Fei et al. 2018). Most of the magnesian skarn rocks are distributed in the exoskarn region near the sedimentary rocks.

4. Samples and analytical methods

Samples for this study were collected from underground mine excavations. Following detailed field investigations and microscopic studies, representative samples of different types of garnets were selected for electron microprobe analyses (EMPA), X-ray element mapping, back scattered electron imaging (BSE), laser ablation–inductively coupled plasma–mass spectrometry (LA-ICP-MS) analyses. The different types of garnets are located along Line *AA'* and *BB'* shown in the geological map (Fig. 2). Detailed analytical methods and processes are described in Appendix 1. Chemical compositions are reported in the supplementary material (Appendix Table).

5 Results

5.1 Garnet morphology

Garnet grains are dominant in calcic skarn, but are less common in the magnesian skarn. Based on optical characters, three types of garnet were identified in the calcic skarn whereas the magnesian skarn contains only one type (Fig. 3).

Garnet in calcic skarn rocks

Type I garnets are characterized by red to orange color (Fig. 3a), dodecahedral and euhedral crystal shape and are fractured (Fig. 3b). Some grains also occur as pectinate aggregates. These garnet grains are anisotropic, and display polysynthetic twinning consisting of four, six (Fig. 3b) or more wedge-shaped sectors radiating from the center of the crystal. Some compositional zoning and polysynthetic twinning are identified, although they are not always consistent within individual grains (Fig. 3d-e). Epitaxial growth with oscillatory zoning on preexisting {110} face is recognized on the boundary (Fig. 3c). Sometimes, the core of type I garnet has been cut by type III garnet.

Type II garnets are anisotropic and show pale yellow color, euhedral to subhedral morphology, occurring as aggregates with oscillatory zoning (Fig. 3f-h). Some type II garnets show oscillatory zoning outside the preexisting dodecahedral type I garnets which were fragmented during the retrograde stage. Some of the cores of type II garnet have been seen replaced by type III garnet.

Type III garnet is yellow and isotropic, and occur as euhedral to subhedral aggregates with oscillatory zoning showing morphological transition from planar dodecahedral {110} crystal faces in the core to composite dodecahedral {110}-trapezohedron {211} crystal faces growth in the margin (Fig. 3i-m). This type of garnet generally replaces pyroxene formed in the prograde stage (Fig. 3j-k) and cut across magnetite that formed in the retrograde stage (Fig. 3l).

Garnet in magnesian skarn rocks

Garnet grains are almost absent in the magnesian skarn rocks. However, some euhedral isotropic grains occur along veins in the prograde stage associated surrounding magnetite grains (Fig. 3n-p, termed as type IV). They occur far from the porphyritic granite and adjacent to the sedimentary wall rocks associated with chalcopyrite-galena-sphalerite orebodies.

5.2 Major element data of garnet

Garnet in calcic skarn rocks

Garnet grains in calcic skarn belong to the grossular-andradite (grandite) solid solution ranging in composition from $Grs_{80}Adr_{15}$ to $Grs_{0.3}Adr_{97}$ with <6 mol.% spessartine, <3 mol.% pyrope and 0.3-10 mol.% almandine (Fig. 4; Appendix 2). Under BSE images, all types of garnets in the calcic skarn rocks exhibit core-rim oscillatory compositional zoning (Fig. 3).

Type I garnet shows considerable variations in composition ($Grs_{18\text{-}80}Adr_{10\text{-}75}$) with 0.1-6 mol.% spessartine and 0.3-4 mol.% almandine, but mostly in $Grs_{50\text{-}80}Adr_{20\text{-}50}$ (Fig. 4; Appendix 2). Most of them show compositional zoning with $Grs_{60\text{-}80}Adr_{20\text{-}40}$ while a small amount of the altered inner zones displays lower grossular (25-50 mol%) and higher andradite (50-75 mol%) (Table 1). Overall, the epitaxial growth with oscillatory zoning in the rim region exhibits notable variations with higher andradite (~60 mol. %) contents and lower grossular contents (~35 mol. %) than in the early formed zones in the relative core region (Appendix 3; Fig. 5). They also display relatively high F contents (<1.54 %, Fig. 6).

Garnet from the type II and type III are Fe-rich and display relatively wide compositional range of $Grs_{0.1\text{-}47}Adr_{30\text{-}97}$. Stoichiometry calculation (Table 1) shows that most of the iron is in oxidized state (Fe^{3+}), resulting in the formation of andradite-rich type II and type III garnets.

Type II garnet shows relatively higher grossular contents and wider compositional range ($Grs_{1\text{-}47}Adr_{30\text{-}95}$) than the type III garnet. Individual type II garnets have relatively small range of compositions (Table 1), with grossular contents less than 27 mol. % (Appendix 3; Fig. 5). Overall, oscillatory zoning is complimented by compositional variations, with increasing andradite contents and decreasing grossular contents from core to rim. Some of the altered inner zones also show notable variations (Fig. 5). Type II garnet displays relatively lower contents of F (<0.27%, Fig. 6).

The type III garnet grains display high andradite contents ($Grs_{0.1-12}Adr_{85-97}$). Garnet crystals of this type exhibit distinct core-rim compositional oscillatory zoning with different crystal faces (Fig. 3j; Fig. 3m). Zoning of trapezohedron {211} crystal faces corresponds to higher andradite (90-95 mol. %) contents than that of {110} crystal faces (80-90 mol. %) in type III garnet (Table 1). Type III garnet shows the lowest content of F (<0.23% with almost less than 0.05%, Fig. 6).

The andradite compositions and F contents in calcic garnet show negative linear relationship (Fig. 6).

Garnet in magnesian skarn rocks

Type IV garnets differ significantly from those in calcic skarn rocks and exhibit considerable variation in composition with 10-23 mol. % grossular, 48-62 mol. % spessartine and 14-29 mol.% almandine (Appendix Table-1). Stoichiometry calculation shows that nearly all of the iron occurs in the reduced state (Fe^{2+}).

5.3 Trace element data of garnet

The LA-ICP-MS analytical data show that different types of garnet have a wide variation in trace element concentrations. However, their large ion lithophile element (LILE), high field strength element (HFSE) and rare earth elements (REE) contents exhibit a consistent variation.

Garnet in calcic skarn rocks

The garnet crystals in calcic skarn rocks exhibit different REE patterns (Appendix Table-2; Fig. 7), although the same types of garnet show similar chondrite normalized REE patterns. Except for one spot which is strongly altered, the type I garnets display strongly negative Eu anomaly (Eu/Eu* of 0.03-0.90) and low REE contents (3.27-78.26 ppm) with strong light REE depletion (LREE, 0.57-44.56 ppm) relative to heavy REE (HREE, 2.31-59.19 ppm). In contrast, type II garnet grains show REE contents of 13.73~377.08 ppm with most of the values falling in the range of 13.73-74.05 ppm (only REE contents of two altered samples exceed 100 ppm). They also display variable Eu anomalies (Eu/Eu* of 0.16-3.34), and transitional REE patterns with slight to moderate LREE enrichment (1.01-191.83 ppm) relative to HREE (0.47-185.25 ppm, Fig. 7). The type III garnet grains containing REE contents of 1.5-52.05 ppm exhibit LREE-enriched (0.80-51.87 ppm) and flat HREE (0.15-2.46 ppm) patterns with markedly positive Eu anomalies (Eu/Eu* of 0.93-27.07 with almost >1).

Type I garnet shows considerable amounts of Sn (533.89-2545.20 ppm) and W (0.76-100.91 ppm) contents (Table 2, Fig. 8a-b). The zoning in polysynthetic twins corresponds to a gradual decrease in W content and an increase in Sn contents from core to rim (Appendix Table-2; Appendix 3). Moreover, W in type I garnets shows a negative relationship with the andradite content whereas Sn and REE exhibit relatively positive relationship (Fig. 8a-b). In contrast, type II garnets with moderate contents of grossular and andradite have the highest Sn (64.36 to 2778.92 ppm) and the lowest W contents (1.11-468.44 ppm). Type III garnet shows a range of

99.17-1941 ppm Sn (Table 2; Fig. 8b). Sn in type III garnet exhibits a negative relationship with andradite content. These garnet grains also possess high W contents (13.18-771.74 ppm) displaying positive relationship with andradite content (Fig. 8a).

The Eu/Eu* versus X_{Adr} diagram displays a parabola shape (Fig. 8e), in which garnet grains having intermediate compositions of grossular and andradite possess the lowest Eu/Eu* ratios (~0.10). The data suggests that Eu in Eu/Eu*>>1 is present as Eu^{2+}, which contrasts with the 3+ state of the other REEs. The $(La/Yb)_N$ versus X_{Adr} relationship also shows a parabola shape possessing a general tendency of elevated LREE/HREE fractionation with increasing Fe- or Al-content (Fig. 8f).

Garnet in magnesian skarn rocks

The type IV garnets are characterized by a steep positive slope from LREE (1.18-3.26 ppm) to HREE (464.56-468.38 ppm) with strongly negative Eu anomaly (Eu/Eu* of 0-0.02) (Appendix Table-2; Fig. 7g). Compared to those in calcic skarn rocks, type IV garnets have lower content of Sn (18.80-119.15 ppm) and W (0.36-1.12 ppm) (Fig. 8a-b).

6 Discussion

6.1 Birefringence of garnet

Grandite in skarn systems is known to exhibit optical anisotropy, undulatory extinction, twinning, and oscillatory zoning (Shore and Fowler 1996; Pollok et al. 2001). These abnormal optical characteristics describe a deviation from the space group Ia3d of the garnet (Becker and Pollok 2002), and several possible factors have been invoked as summarized below.

1) External stress imparted by tectonic activities in region (McAloon and Hofmeister 1993); 2) oscillatory compositional variations in Ca-Fe-Mn-Mg ordering of the X-site divalent cations in the dodecahedral position (Wang et al. 2000); 3) oscillatory compositional variations in Al-Fe ordering of the Y-site trivalent cations in the octahedral site (Griffen et al. 1992); 4) local strain of structural distortion caused by localized cation substitution when the ionic radii between host and substitute differ significantly in size (e.g., REE for Ca in the X-site) (Ballaran et al. 1999); 5) REE incorporation into the X-site causing magneto-optic effects (Gaspar et al. 2008); 6) hydrogrossular substitution, with ordering of OH or F groups (Rossman and Aines 1991; Manning and Bird 1990); and 7) strain developed in garnet crystal from lattice mismatch at compositional bands, twinning planes or grain boundaries induced by kinetics (Becker and Pollok 2002; Antao and Klincker 2013; Lessing and Standish 1973; Chase and Lefever 1960).

The three types of garnets together with their mineral assemblages in the calcic skarn rocks of present study exhibit no evident deformation or undulatory extinction. Previous studies noted that garnet formed in deformed metamorphic rocks displays slight or no anisotropy, excluding the external factors as the main reason (Hofmeister et al. 1998). Furthermore, the garnet twinning or garnet zoning anisotropy does not display any consistent patterns with the fractures in the mineral. In addition, the twin crystal of type I garnet cuts across the crystal face of the garnet. Under cross-polarized light, oscillatory zoning shows fine-scale, straight and distinct character. These features suggest that birefringence of garnet is unlikely triggered by external stress during growth of garnet.

As described above, the garnets in the calcic skarn rocks are all calcic garnet with only minor Fe^{2+}, Mn and Mg. The Mn content in calcic garnet (0-0.171 in atoms per formula unit with an average of 0.056) is slightly higher than those of the Fe^{2+} and Mg (Table 1). Two-dimensional scan images (Fig. 5) suggest that the distribution of Mn in garnet grains is inconsistent with optical anisotropy. Moreover, as mentioned by McAloon and Hofmeister (1993), dodecahedral ordering cannot cause birefringence. Becker and Pollok (2002) reported miscibility gaps between grossular and grandite, and between grandite and andradite below ~ 430 K based on transmission electron microscopy (TEM) indicating that grandites can have an Al/Fe^{3+} ordered structure below 430 K. However, Barkoff et al. (2017) estimated that the temperature of most of the skarn deposits is above 600 K, which is much higher than the miscibility temperature of grossular-andradite. The BSE and two-dimensional scan images (Fig. 3; Fig. 5) show that most isotropic type III garnet is characterized by compositional zoning as anisotropic type I and type II garnets, and the compositional zoning in type I garnet grains is prevalent across the twinning sectors, with different extinction characters. Therefore, we exclude hypotheses (2) and (3).

Moretti and Ottonello (1998) mentioned that garnet with REE content exceeding a few hundred ppm of bulk is more likely to induce polyhedral distortion. However, Hofmeister et al. (1998) found that synthetic garnets containing stoichiometric REE (e.g., $Y_3Fe_5O_{12}$) has only weakly optical birefringence based on experimental work. The anisotropic garnet (type I and type II) has wide variation in REE composition

(3.27-377.05 ppm, with most of the values in the range of 3.27-78.26 ppm except two samples), whereas isotropic garnets contain REE contents of 1.5-52.02 ppm (Fig. 8d, Appendix Table-2). As for the type I with polysynthetic twinning, the REE distribution is inconsistent with the anisotropic sections, excluding the possibility of REE-induced anisotropism in polysynthetically twinned type I garnet. Additionally, many of the anisotropic type II and isotropic type III garnet grains also display relatively similar REE contents. Therefore, we exclude hypotheses (4) or (5) as the main factor.

Based on the EMPA results and two-dimensional scan images (Fig. 5), we infer that the F content does not have any correlation with twinning or oscillatory zoning. Therefore, anisotropy cannot have been caused by hydrogrossular substitution, which excludes hypothesis (6).

The EMPA results together with two-dimensional scan images (Appendix Table-1, Fig. 5) suggest that most of the anisotropically zoned domains have the composition: $Grs_{20-60}Adr_{40-80}$, whereas the type I and type III garnet compositional zoning possess higher end member contents. These features are consistent with anisotropic zoned garnet compositions reported by other workers (e.g., Xu et al. 2016; Gaspar et al. 2008; Sepidbar et al. 2017). The ionic size of Fe^{3+} and Al^{3+} differ appreciably (0.6655 Å Fe^{3+} of and 0.5350Å of Al^{3+}, Ottonello et al. 1996; Moretti and Ottonello 1998). When the garnet has an intermediate composition, the substitution in garnet lattice may require relatively larger stress to generate the observed anisotropism than in the case of garnets with higher end-member contents. Moreover, as for twin planes in anisotropic type I garnet, the compositional zoning and polysynthetic twinning do not always overlap, which infer that the anisotropy of type I garnet may be caused by strain form lattice mismatch at twin boundaries. Therefore, we conclude that the birefringence of garnet is probably caused by strain from lattice mismatch in twinning boundary or banding substitution with garnets containing intermediate composition of grossular-andradite.

6.2 Garnet oscillatory zoning

The BSE images together with two-dimensional compositional images show that almost all garnet types in calcic skarn rocks possess consistent oscillatory compositional zoning patterns and can be observed from core to rim regions (Fig. 3; Fig. 5).

According to the width of the zones, Downes (1974) divided oscillatory zoning into two types: fine banding (1-10 μm) and coarse banding (1-100 mm). These two types of bandings have been generally considered to be of different origin (Streck 2008). The sharp, fine and adjacent garnet zoning patterns in between are all within 1 μm, classifying as fine banding type (Fig. 3). Two models have been proposed for the formation of the fine banding type of oscillatory zoning in garnet. One is by internal control caused by the following two processes. 1) Self-organization (e.g., Holten et al. 1997; Shore and Fowler 1996; Pollok et al. 2001) in which the minerals are under supersaturation, and the mineral growth rate is higher than the mineral diffusion rate leading to locally disequilibrium. 2) Immiscibility in the grossular-andradite (grandite) system (Jamtveit 1991). Alternate mechanisms involving changes of externally controlled growth conditions such as temperature, f_{O2}, pH and salinity (Yardley et al. 1991; Jamtveit et al. 1995) or dynamic changes in the magmatic-hydrothermal system (Ginibera et al. 2002; Ciobanu and Cook 2004; Streck 2008) has also been proposed. In this case, the garnet and external factors are under near-equilibrium conditions in a local domain, and the oscillatory zoning indicates the changes in the external environment.

As discussed above, experimental studies together with computational results show that there are miscibility gaps between grossular and grandite when the temperature is ≤430K, which is too low to produce oscillatory zoning, even on a geological time-scale (Becker and Pollok 2002; Pollok et al. 2001). There is no garnet miscibility gap in the Cuihongshan deposit (Fig. 4). Hence, the grossular-andradite system is unlikely to be induced by immiscibility.

There is a consensus that external factors can influence the composition of garnet (Gaspar 2008; Jamtveit et al. 1993, 1995). The fluctuations in Al/Fe ratios of the pore fluid can be caused by variable rates of infiltration and kinetic dispersion in the skarn system (Cionabu and Cook 2004). Based on the BSE and element mapping images (Fig. 3, 5), it is evident that the garnet exhibits higher andradite and lower grossular compared rim zones with core zones. We correlate with feature with the external factors, especially the composition of the hydrothermal system. The different garnet types formed in distinct stages and coexisted with different mineral assemblages also suggest that the garnet composition was driven by the external factors.

Regarding the distinct fine-scale, sharp and adjacent zoning in garnet, Holten et al. (1997, 2000) proposed that similarity in intracrystalline zoning does not necessarily imply that the zoning pattern was produced by changes in the external conditions. Streck (2008) suggested that fine zonation may be largely kinetically controlled whereas coarse zoning reflects dynamic processes, which also implies that the oscillatory zoning is caused by self-organization related to kinetic effects. Additionally, Lessing and Standish (1973) suggested that narrow zoning with sharp contacts correspond to rapid crystal growth and/or rapid changes of composition in the hydrothermal system in order to preserve these delicate lamellae. Rapid changes of hydrothermal fluid composition may cause gradual composition variations in garnet growth zones. However, the BSE and element mapping images (Fig. 3, 5) show that the chemical variations in calcic garnet grains are not gradual, but abrupt, and thus further support a relatively rapid isolation of crystallizing garnet from the hydrothermal solutions (Jamtveit 1991; Smith et al. 2004). Moreover, Ciobanu and Cook (2004) emphasized the role of surface kinetics together with local transport processes near crystal surface, invoking garnet self-organization mechanisms to account for the minor variations in garnet compositions. We therefore infer that internal self-organization has played a significant role in the formation of these sharp, fine and closely spaced garnet zones. These zoning patterns and the marked variations in garnet composition were possibly controlled by external factors.

6.3 REEs in garnet

6.3.1 Substitution of REE into garnet

Based on the ionic radii together with garnet crystal radii for elements in garnet structure (Shannon 1976), the only possible replacement of REE is substitution of X site in the dodecahedral position. However, substituting REE^{3+} has a different charge than the ion normally occupying the X^{2+} site. The charge imbalance must be compensated either through a coupled substitution or the creation of a vacancy. In general, the following five mechanisms have been proposed to explain the incorporation of REE into garnets.

1) Yttrogarnet (YAG)-type substitution involving charge balance by substitution of a trivalent cation (e.g., Fe^{3+}, Al^{3+}) into the Z (Si) site (Jaffe 1951; Ding et al. 2018); 2) incorporation of a monovalent cation (e.g. Na+) into the X site forming Na^{+}-REE^{3+} couple substitutions (Enami et al. 1995; Sepidbar et al. 2017); 3) change in compensation via vacancies in the dodecahedral site (Ismail et al. 2014); 4) substitution of divalent cations (e.g. Mg^{2+}; Fe^{2+}) into the Y site (menzerite-type, Carlson 2012; Grew et al. 2010); and 5) substitution of F^{-} or OH^{-} into the Si-O tetrahedron (Jamtveit and Harvig 1994; Gross 2008).

Our EMPA results show that garnet grains in the Cuihongshan deposit have low Na concentrations (Table 1), indicating that these did not undergo Na^{+}-REE^{3+} coupled substitutions. Although the garnet grains contain some F the variation between REE and X_{Adr} is not consistent with the relation between F and X_{Adr}, suggesting that the F^{-}-REE^{3+} coupled substitution mechanism is unlikely.

Additionally, the primary criterion for distinguishing substitution of divalent cations (e.g. Mg^{2+}; Fe^{2+}) into the Y site is the dominance of divalent cations with Mg>Fe^{2+} under pressures of 7-8.5 kbar and temperatures of 700-800°C (Carlson 2012;

Grew et al. 2010). This would suggest that the substitution of divalent cations (e.g. Mg^{2+}; Fe^{2+}) into the Y site mechanism in the skarn system of our study is unlikely.

Thus, we suggest that garnet grains in the Cuihongshan deposit favored a YAG type substitution. However, the mechanisms involving the creation of structural vacancies are difficult to evaluate (Sepidbar et al. 2017).

6.3.2 REE in garnet

Pyrope-grossular garnet solid solutions exhibit strong deviations from ideal mixing in their thermodynamic properties (Du et al. 2017, 2015). Deviations from ideal behavior tend to be greater in solutions with high ionic strength, especially hydrothermal and ore-forming fluids (White 2013). As a result, we assume that the grossular-andradite garnet solid solution displays an asymmetric model. The Gibbs free energy change of this non-ideal binary solution is given by:

$$\Delta G^{VI} = nRT\left(x_{grossular}\ln x_{grossular} + x_{andradite}\ln x_{andradite}\right) + \Delta G_{excess} \qquad (1)$$

Where $x_{grossular}$ and $x_{andradite}$ are the mole fractions of the respective components of the garnets, T is the temperature in the hydrothermal system, R is the molar gas constant (8.314 J· $mol^{-1}\cdot K^{-1}$), n=2 based on the garnet chemical formula of $X_3Y_2Z_3O_{12}$.

A two-parameter Margules fit was adopted with the molar volume values of garnet (Engi and Wersin 1987). Thus, the excess free energy change in this binary solution is given by:

$$\Delta G_{excess} = n x_{grossular} RT\ln\gamma_{grossular} + n x_{andradite} RT\ln\gamma_{andradite} =$$
$$n\left(\omega^{G}_{grossular} x_{andradite} + \omega^{G}_{andradite} x_{grossular}\right) x_{grossular} x_{andradite} \qquad (2)$$

where

$$\mathrm{RTln}\gamma_{\mathrm{grossular}} = [\omega^{\mathrm{G}}_{\mathrm{grossular}} + 2(\omega^{\mathrm{G}}_{\mathrm{andradite}} - \omega^{\mathrm{G}}_{\mathrm{grossular}})x_{\mathrm{grossular}}]x^{2}_{\mathrm{andradite}} \quad (3)$$

$$\mathrm{RTln}\gamma_{\mathrm{andradite}} = [\omega^{\mathrm{G}}_{\mathrm{andradite}} + 2(\omega^{\mathrm{G}}_{\mathrm{grossular}} - \omega^{\mathrm{G}}_{\mathrm{andradite}})x_{\mathrm{andradite}}]x^{2}_{\mathrm{grossular}} \quad (4)$$

$\omega^{\mathrm{G}}_{\mathrm{grossular}}$ and $\omega^{\mathrm{G}}_{\mathrm{andradite}}$ are the excess Gibbs parameters in the Margules formation.

Regarding the incorporation of REE in garnet, previous studies have shown that mixing of REE garnet components below about a few hundred ppm with major silicate garnet components is virtually ideal, which is the region where Henry's law holds (Moretti and Ottonello 1998).

$$\mu_{\mathrm{REE}} = \mu^{0}_{\mathrm{REE}} + \mathrm{RTln}x_{\mathrm{REE}}\gamma_{\mathrm{REE}} = \mu^{*}_{\mathrm{REE}} + \mathrm{RTln}x_{\mathrm{REE}} \quad (5)$$

Where μ_{REE} is the chemical potential, which is simply the partial molar Gibbs free energy, γ_{REE} is independent of x_{REE} in the hydrothermal fluid at constant T and P and can be considered as adding or subtracting a fixed amount to the standard state chemical potential, and μ^{*}_{REE} is obtained by extrapolating the Henry's law slope to $x_{\mathrm{REE}}=1$ at the chemical potential.

The divalent cations (Ca, Mg, Mn, Fe^{2+}, K^{+}, Na^{+}) in eightfold coordination $x_{\mathrm{divalent}}\rightarrow 1$, the μ_{divalent} should reduce to Raoult's law.

$$\mu_{\mathrm{divalent}} = \mu^{0}_{\mathrm{divalent}} + \mathrm{RTln}x_{\mathrm{divalent}} \quad (6)$$

$$\Delta\mathrm{G}_{\mathrm{sol}} = \Delta\mathrm{G}_{\mathrm{divalent}} + \Delta\mathrm{G}_{\mathrm{REE}} = \mathrm{n'RT}x_{\mathrm{divalent}}\mathrm{ln}x_{\mathrm{divalent}} + \mathrm{n'RT}x_{\mathrm{REE}}\mathrm{ln}x_{\mathrm{REE}}\gamma_{\mathrm{REE}} \quad (7)$$

Hence, ΔG in the grossular-andradite system relative to the pore end member composition is

$$\Delta\mathrm{G} = \Delta\mathrm{G}^{\mathrm{VI}} + \Delta\mathrm{G}_{\mathrm{sol}} = \mathrm{nRT}\left(x_{\mathrm{grossular}}\mathrm{ln}x_{\mathrm{grossular}} + x_{\mathrm{andradite}}\mathrm{ln}x_{\mathrm{andradite}}\right) +$$

$$\mathrm{n}\left(\omega^{\mathrm{G}}_{\mathrm{grossular}}x_{\mathrm{andradite}} + \omega^{\mathrm{G}}_{\mathrm{andradite}}x_{\mathrm{grossular}}\right)x_{\mathrm{grossular}}x_{\mathrm{andradite}} + \mathrm{n}'\mathrm{RT}x_{\mathrm{divalent}}\ln x_{\mathrm{divalent}} + \mathrm{n}'\mathrm{RT}x_{\mathrm{REE}}\ln x_{\mathrm{REE}}\gamma_{\mathrm{REE}} \quad (8)$$

From the discussion above, ΔG^{VI} is controlled by the relative components between grossular and andradite whereas ΔG_{sol} is broadly related to the component of REEs and divalent cations. Most of the garnets in the Cuihongshan deposit contain $X_{\mathrm{REE}} \leq 10^{-3.3}$, which results in negligible values of ΔG_{sol} suggesting that ΔG is mostly depended on ΔG^{VI} in the garnet grains of the skarn system. Moreover, low concentrations of REE contents (10^{-3}-10^{-4} ppm) suggest ideal solid solution, which indicate that incorporation of REE is controlled by the ΔG as a function of ionic fraction of the garnet component. According to this interpretation, the concentration of REEs is mainly related to the relative components of grossular and andradite.

On the basis of equation (1), the ΔG in grossular-andradite solid solution is mostly determined by temperature of the system, $x_{\mathrm{grossular}}$, $x_{\mathrm{andradite}}$, $\omega^{\mathrm{G}}_{\mathrm{andradite}}$ and $\omega^{\mathrm{G}}_{\mathrm{grossular}}$. If the temperature of the system remains constant and $\omega^{\mathrm{G}}_{\mathrm{andradite}} = \omega^{\mathrm{G}}_{\mathrm{grossular}}$, ΔG becomes the lowest when $\mathrm{x}_{\mathrm{grossular}} = \mathrm{x}_{\mathrm{andradite}} = 0.5$. It is well established that temperature of the skarn system will gradually decrease during the formation of the mineral deposit, which will increase ΔG in the system. If the solution model were symmetric, the lowest ΔG would appear at approximately $\mathrm{x}_{\mathrm{grossular}} > 0.5$ and $\mathrm{x}_{\mathrm{andradite}} < 0.5$ leading to the highest REE contents at this point. However, from the REE versus X_{Adr} diagram (Fig. 8d), garnet with ~20% grossular and 80% andradite commonly shows the highest REE content, linking this solid solution to an asymmetric model. Engi and Wersin (1987) described the grossular-andradite solid solution with an asymmetric Margules model based on phase equilibrium data from Huckenholz and Fehr (1982). The Margules equation is an interaction parameter since non-ideal behavior arises from interactions between molecules or atoms and depends on temperature, pressure, and the nature of the solid solution except composition (White 2013). As a result, the non-ideal behavior in the grossular-andradite solid solution system may be related to the size mismatch between Al^{3+} (0.535) and Fe^{3+} (0.6655) (Ottonello et al. 1996; Moretti and Ottonello 1998) or the neighbor interactions or coordination on the X-O and Y-O site (van Westrenen et al. 2003). Moreover, the non-ideal mixing properties such as enthalpy, volume, free energy, and vibrational entropy are not only dependent on the complex crystal structure caused by Fe and Al substitution but also the mechanism by which the garnet lattice accommodates different size of Fe and Al in the solid solution. However, because of the presence of Fe^{2+} in dodecahedral sites due to the valence states of Fe, incorporation of F^- and OH^- due to the hydrogarnet substitution and incorporation of Fe^{3+} and Al^{3+} into the SiO_4 tetrahedron site due to the YAG-type substitution discussed above, the Gibbs energy calculation of this asymmetric solid solution becomes more complex.

Regarding the calculation of ΔG, we suggest that the relative proportion of grossular towards andradite in the solid solution together with temperature in the system has influenced the garnet REE concentrations. The grossular-andradite solid solution exhibits an asymmetric model.

6.3.3 REE fractionation in garnet

The trace element geochemistry of garnet in the Cuihongshan skarn deposit shows a prominent REE fractionation with grossular displaying LREE-depletion and HREE-enrichment, together with a general negative Eu anomaly. In contrast, the andradite shows LREE-enriched and HREE-depleted feature with a general positive and variable Eu anomaly (Fig. 7).

Several possible factors can be considered to explain these features, as listed below.

1) Different substitution mechanisms between the LREEs and the HREEs which may be caused by the ionic radii and garnet crystal radii for elements relevant in garnet chemistry (Ding et al. 2018); 2) the concentration of the elements in the liquid from which grossular and andradite crystallized has significantly changed (Ismail et al. 2014; Ranjbar et al. 2016; Zhao et al. 2016); 3) different partition coefficients of the REEs between grossular and andradite end-member garnets; 4) external factors such as temperature and pressure; and 5) the relative composition of the andradite-grossular solid solution lead to different REE fractionation character.

From the discussion above, incorporation of REEs into garnets favor a YAG-type substitution ($(Ca_{1-y}REE_y)_3Al_2(Si_{1-y}Al_y)_3O_{12}$ and $(Ca_{1-y}REE_y)_3Fe_2(Si_{1-y}Fe_y)_3O_{12}$). Compared with the garnet crystal radii and ionic radii, the radii of LREEs are more comparable to that of Ca than HREEs in the dodecahedral site (Ottonello et al. 1996; Moretti and Ottonello 1998). However, based on the garnet REE patterns of grossular and andradite (Fig. 7), we consider that this mechanism is not the main cause.

In order to estimate the REE patterns, we take into account the prograde minerals that formed first from magmatic-hydrothermal fluids. From Fei et al. (2018), the REE patterns of skarn-related granite suggest that the magmatic-hydrothermal system was gradually enriched in LREE and depleted in HREE as compared to less evolved granites, suggesting a LREE-enriched and HREE-depleted magmatic-hydrothermal system. This contrasts with the REE patterns of garnet forming at the prograde stage. Hence, we infer that the compositional variation of hydrothermal fluid is not the main factor that controlled the REE fractionation patterns in Cuihongshan skarn deposit or other similar hydrothermal deposits.

Regarding hypothesis (3), Moretti and Ottonello (1998) reported $La_3Fe_5O_{12}$, $Lu_3Fe_5O_{12}$, $La_3Al_5O_{12}$ and $Lu_3Al_5O1_2$ that show LREE-depleted and HREE-enriched characters. Gaspar et al. (2008) calculated the H_{mixing} of LaFeG-Adr, LuFeG-Adr, LaAlG-Grs and LuAlG-Grs and found that garnets exhibit LREE-depleted and HREE-enriched patterns when their REE contents are negligible. Thus, we suggest that the end-member of grossular-andradite solid solution do not exhibit different REE patterns in the skarn system.

Regarding hypothesis (4), experimental studies show that although the temperature and pressure exert significant influence the REE content, these parameters have limited influence on the garnet REE fractionation (Gaspar et al. 2008). Previous studies have calculated the REE fractionation of garnet under 300°C, 400°C and 500°C at pressures of 1 kbar and 5 kbar, respectively (Appendix 4). Based on these experimental studies, both end-members of grossular and andradite show LREE-depleted and HREE-enriched REE patterns. The results suggest that REEs, especially HREEs are more compatible in both grossular and andradite, suggesting that the above process is not the main cause.

In this study, we prefer hypothesis (5) which suggests that the relative composition of grossular-andradite solid solution controls the LREE-HREE fractionation in garnet skarns.

For a finite change at constant temperature, the Gibbs free energy in the system is:

$$\Delta G_{\mathrm{real\ mixing}} = \Delta H_{\mathrm{excess}} + \mathrm{nRT}\sum_{\mathrm{i}} \mathrm{X_i} \ln \mathrm{X_i} - \mathrm{T}\Delta S_{\mathrm{excess}} \qquad (10)$$

It is obvious that the relative content of grossular-andradite solid solution together with temperature in the same stage can be regarded as constant. Additionally, the content of LREE together with HREE is below several hundred ppm indicating that the mixing of REE in silicate garnets is virtually ideal. Thus, ΔS has little effect on the system. Gaspar et al. (2008) calculated the excess enthalpy for garnet solid solutions (Appendix 5). The enthalpy of excess for $\mathrm{LuGrs_{0.5}Adr_{0.5}}$ is lower than that of $\mathrm{LaGrs_{0.5}Adr_{0.5}}$ when $\log X_{\mathrm{REE,VIII}}<1$ and display opposite characters when $\log X_{\mathrm{REE,VIII}}$ exceed $10^{-3.5}$. The enthalpy of excess for $\mathrm{LaGrs_{0.1}Adr_{0.9}}$ is evidently lower than that of $\mathrm{LuGrs_{0.1}Adr_{0.9}}$, respectively, displaying marked difference from the end members. This result is consistent with our data from the Cuihongshan skarn deposit and other skarn deposits such as the Hongniu-Hongshan Cu skarn deposit (Peng et al. 2016), skarns on the Isle of Skye (Smith et al. 2004) and Tongling Cu-S-Fe-Au skarn deposit (Zhang et al. 2017).

Moreover, when evaluating the REE contents in the garnet during different mineralization stages, ΔS shows significant change. The relative composition of grossular-andradite has influenced ΔS and temperature has gradually decreased during the ore formation. Combining the enthalpy of mixing of $Grs_{0.5}Adr_{0.5}$ is significantly lower than that of $Grs_{0.1}Adr_{0.9}$, and the ΔG of $Grs_{0.5}Adr_{0.5}$ is lower than that of $Grs_{0.1}Adr_{0.9}$. This result is consistent with previous discussion.

6.4 Relative component of grossular-andradite in the solid solution

In the grossular-andradite solid solution, if G_{real} is less than $G_{mixutre}$, a solution is stable relative to pure phase. Moreover, as discussed above, garnet with approximate 20% grossular and 80% andradite commonly displays the lowest G_{real}, suggesting that $Grs_{20}Adr_{80}$ is the most stable phase (Fig. 8c-d). However, the andradite contents from the early to the late stage show gradual increase, whereas the grossular content show decrease based on the compositional variations in different types of garnet growing different mineralogy stages (Fig. 4; Appendix 2). Towards the late retrograde stage, type III garnet is almost pure andradite. Furthermore, it is evident that the rim contains more andradite and less grossular components in the zoned garnet (Fig. 5).

The relative concentrations of Fe and Al in garnet depend on the following factors:

1) the concentration of the element in the liquid from which it crystallizes; 2) whether other Al- and Fe-bearing minerals crystallizing at the same time are competing for those elements; and 3) external conditions such as temperature, pressure and f_{O_2}.

As described above, when Fe-rich type III garnet crystallized from the hydrothermal fluid, magnetite crystallized at the same time which competes for iron. We therefore, exclude hypothesis (2). It is indeed possible that the external factors changed during the growth of garnets. However, as discussed above, decreasing temperature in the system would increase ΔG whereas decreasing f_{O_2} would decrease Fe^{3+} formation in the hydrothermal system, thus not favoring andradite formation. In this way, we exclude hypothesis (3).

Hence, the compositional variation of grossular-andradite would mostly depend on the content of these elements in the hydrothermal fluid. It is consistent with discussion above that the oscillatory zoning patterns in neighbor result from local nonlinearities in the growth process of garnet whereas the evidently compositional variations from core to rim might have been caused by the composition of hydrothermal fluids. Further, we infer that the relative composition of Fe^{3+} and Al^{3+} has changed in the fluid during the formation of different types of garnets in the calcic skarn rocks. In this way, although the REE component in garnet cannot provide information on the hydrothermal fluids, the major component in the garnet solid solution demonstrates that during the retrograde stage, the Fe^{3+}/Al^{3+} in the hydrothermal skarn has increased.

6.5 W and Sn in garnets as an indicator for W-Sn deposit exploration

Although REE, HFSE, U and Th are easily enriched in hydrothermal and metamorphic garnets, granitophile elements (W, Sn and Mo) are not commonly concentrated in skarn garnet garnets (Chen et al. 2015; Xu et al. 2016). Park et al. (2018) noted that granitophile elements are important in constraining skarn-forming processes. Garnet grains in the Cuihongshan deposit also show significant contents of Sn and W, the concentration of which is sometimes as high as several thousands of ppm (Appendix Table-2; Fig. 8a-b). However, previous studies have suggested different concentration characteristics between W, Sn and garnet (Park et al. 2018; Xu et al. 2016). The garnet in Cuihongshan deposit shows a continuous compositional range, without any gap, which is a useful feature to address the accurate concentration patterns of the "granitophile" elements (Mo, W and Sn, Xu et al. 2016). As shown in Fig. 8a-d, the concentrations of Sn and W exhibit different features as compared with REE. This aspect is further discussed below.

W in garnet

The ionic radius of W^{6+}(0.68Å) is similar with Fe^{3+}(0.645 Å) and Al^{3+}(0.535Å) indicating that incorporation of W is only possible by replacement of Y site in the octahedral position. As described previously, the contents of W gradually decrease from type I to type II garnet which owns the lowest W values. The scheelite together with type I garnet has formed during prograde stage, which indicates that the precipitation of W-bearing minerals evidently resulted in a decrease of W in hydrothermal fluids consistent with the latterly formed W-poor type II garnets. This might indicate that the behavior of W in garnet is determined by the W contents in hydrothermal fluid (Fig. 8a). W-bearing garnets have also been found in deposits such as Zhibula copper deposit, Wondong W skarn deposit and Sangan skarn deposit (Xu et al. 2016; Park et al. 2017, Sepidbar et al. 2017). They have shown that W skarn deposits commonly contain various F-bearing minerals such as fluorite, apatite and vesuvianite and indicate a strong petrogenetic link between F content and W enrichment in hydrothermal skarn system (Zaw and Singoyi 2000; Guo et al. 2016). The F-bearing minerals occurring commonly in the Cuihongshan deposit might be related to the enrichment of W in the hydrothermal fluid. However, according to the

W versus X_{Adr} and F versus X_{Adr} plots in the garnet grains (Fig. 6, 8), it is noted that these two elements exhibit extremely different tendency with increasing andradite content. Therefore, we infer that the substitution of W into garnet has no evidently relationship with substitution of F in garnet, which suggest that the F may affect W via influencing the physical-chemical conditions of the hydrothermal system, leading to the consistent formation and precipitation character between W-bearing garnet and scheelite.

Sn in garnet

The ionic radius of Sn^{4+} (0.71Å) is similar with that in Y-site, indicating that incorporation of Sn is possible only by the replacement of Y site cations. Our LA-ICP-MS data reveal that the prograde stage type I garnet crystals in the Cuihongshan polymetallic deposit have elevated Sn contents which appear to be the significant carrier of tin before cassiterite precipitation in the retrograde stage (Appendix Table-2; Fig. 8b). Subsequently, tin is released by precipitation of tin-bearing minerals especially cassiterite. From the Sn versus X_{Adr} diagram, the Sn values in garnet have decreased abruptly from type II to type III garnet (Fig. 8b), consistent with cassiterite precipitation. Therefore, we suggest that the concentration of Sn in hydrothermal fluid is significantly influenced the behavior of Sn during garnet formation than just simply controlled by Fe behavior in garnet and shows a positive relationship with andradite as suggested in previous studies (Park et al. 2018; Ding et al. 2018). Moreover, F-rich fluids have a greater potential to transfer Sn in the hydrothermal system which may lead to the enrichment of Sn in hydrothermal fluids as well (Guo et al. 2016). Besides, Sn and F in the Cuihongshan garnets do not exhibit any evident tendency with increasing andradite contents (Fig. 6; 8), which exclude the possibility that F influenced Sn via substitution of Sn^{4+}-F^{-} in the structure.

Accordingly, we consider that the contents of W and Sn in garnets can be used as indicators for W-Sn deposit exploration in conjunction with the geological features and physicochemical conditions of the ore deposit.

7 Implications

Birefringence in garnet such as oscillatory zoning and twin in hydrothermal systems are probably controlled by the strain from lattice mismatch at substitution and twin. The oscillatory zoning may be a result of the internal self-organization in the growth process of garnets. Thus, this can interpret why oscillatory zoning of garnet is common in skarn system. In this way, crystal morphology in garnet does not indicate the composition variations in the hydrothermal system. However, the composition variations between core and rim in single garnet grains and different types of garnet do imply the concentration character of the hydrothermal system, which indicate that the relative component or Fe^{3+}/Al^{3+} has changed obviously in hydrothermal processes. Moreover, in the W-, Sn- and Mo-bearing skarn deposit, the W and Sn concentration in garnet is a function of the concentration of elements in the hydrothermal fluids, and may be used as an indicator for W-Sn deposit exploration. Hence, the relative components of grossular and andradite as well as “granitophile” elements (Mo, W and Sn) in garnet can reflect the mineralization environment. On the other hand, grossular-andradite garnet solid solution also exhibits strong deviations from ideal mixing in their thermodynamic properties. The concentration of REEs is mainly related to the relative components of grossular and andradite in this solid solution, and REE fractionation of garnet can be attributed to significant Gibbs energy difference between LREE and HREE.

Acknowledgements

This work was financially supported by the National Key Research and Development Program of China (No. 2016YFC0600502) and the 973 program (2012CB416802). We are grateful to Xin Guangde, engineer of the Cuihongshan mining company for his guidance during our field trip.

References

Antao, S.M., and Klincker, A.M. (2013) Origin of birefringence in andradite from Arizona, Madagascar, and Iran. Physics and Chemistry of Minerals, 40, 575-586.

Baghban, S., Hosseinzadeh, M.R., Moayyed, M., Mokhtari, M.A.A., Gregory, D.D., and Mahmoudi, N.H. (2016) Chemical composition and evolution of the garnets in the Astamal Fe-LREE distal skarn deposit, Qara-Dagh–Sabalan metallogenic belt, Lesser Caucasus, NW Iran. Ore Geo. Reviews, 78, 166-175.

Ballaran, T.B., Carpenter, M.A., and Geiger, C.A. (1999) Local structural heterogeneity in garnet solid solutions. Physics and Chemistry of Minerals, 26, 554-569.

Barkoff, D.W., Ashley, K.T., and Steele-MacInnis, M. (2017) Pressures of skarn mineralization at Casting Copper, Nevada, USA, based on apatite inclusions in garnet. Geology, 45, 947-950.

Becker, U., and Pollok, K. (2002) Molecular simulations of interfacial and thermodynamic mixing properties of grossular-andradite garnets. Physics and Chemistry of Minerals, 29, 52-64.

Carlson, W.D. (2012) Rates and mechanism of Y, REE, and Cr diffusion in garnet. American Mineralogist, 97, 1598-1618.

Chase, A. B., and Lefever, R. A. (1960) Birefringence of synthetic garnets. American Mineralogist, 45, 1126-1129.

Chen, Y. X., Zhou, K., Zheng, Y. F., Chen, R. X., and Hu, Z. (2015) Garnet geochemistry records the action of metamorphic fluids in ultrahigh-pressure dioritic gneiss from the Sulu orogeny. Chemical Geology, 198, 46-60.

Ciobanu, C.L., and Cook, N.J., (2004) Skarn textures and a case study: the Ocna de Fier-Dognecea orefield, Banat, Romania. Ore Geology Reviews, 24, 315-370.

Ding, T., Ma, D., Lu, J., and Zhang, R. (2018) Garnet and scheelite as indicators of multi-stage tungsten mineralization in the Huangshaping deposit, southern Hunan province, China. Ore Geology Reviews, 94, 193-211.

Downes, M.J. (1974) Sector and oscillatory zoning in calcic augites from M. Etna, Sicily. Contributions to Mineralogy and Petrology, 47, 187-196.

Du, W., Clark, S.M., and Walker, D. (2015) Thermo-compression of pyrope-grossular garnet solid solutions: non-linear compositional dependence. American Mineralogist, 100, 215-222.

Du, W., Walker, D., Clark, S.M., Li, X., and Li, B. (2017) Microscopic strain in a grossular-pyrope solution anti-correlates with excess volume through local Mg-Ca cation arrangement, more strongly at high Ca/Mg ratio. American Mineralogist, 102, 2307-2316.

Einaudi, M.T., and Burt, D.M. (1982) A special issue devoted to skarn deposits. Introduction – terminology, classification, and composition of skarn deposits. Economic Geology, 77, 745-754.

Enami M., Cong, B., Yoshida, H., and Kawabe, I. (1995) A mechanism for Na incorporation in garnet: an example from garnet in orthogneiss from the Su-Lu terrane, eastern China. American Mineralogist, 80, 475-482.

Engi, M., and Wersin, P. (1987) Derivation and application of a solution model for calcic garnet. Schweizerische Mineralogische und Petrographische Mitteilungen, 67, 53-73.

Fei, X., Zhang, Z., Cheng, Z., Santosh, M., Jin, Z., Wen, B., Li, Z., and Xu, L. (2018) Highly differentiated magmas linked with polymetallic mineralization: A case study from the Cuihongshan granitic intrusions, Lesser Xing'an Range, NE China. Lithos, 302-303, 158-77.

Gaspar, M., Knaack, C., Meinert, L.D., and Moretti, R. (2008) REE in skarn systems: a LA-ICP-MS study of garnets from the Crown Jewel gold deposit. Geochimica et Cosmochimica Acta, 72, 185-205.

Ginibera, C., Kronz, A., Wörner, G. (2002) High-resolution quantitative imaging of plagioclase composition using accumulated backscattered electron images: new constraints on oscillatory zoning. Contributions to Mineralogy and Petrology, 142, 436-448.

Grew, E.S., Marsh, J.H., Yates, M.G., Lazic, B., Armbruster, T., Locock, A., Bell, S.W., Dyar, M.D., Bernhardt, H-J., and Medenbach, O. (2010) Menzerite-(Y), a new species, $\{(Y, REE)(Ca, Fe^{2+})_2\}[(Mg, Fe^{2+})(Fe^{3+}, Al)](Si_3)O_{12}$, from a felsic granulite, Parry Sound, Ontario, and a new garnet end-member, $\{Y_2Ca\}[Mg_2](Si_3)O_{12}$. Canadian Mineralogist, 48, 1171-1193.

Griffen, D.T., Hatch, D.M., Phillips, W.R., and Kulaksiz, S. (1992) Crystal chemistry and symmetry of a birefringent tetragonal pyralspiter$_{75}$-grandite$_{25}$ garnet. American Mineralogist, 77, 399-406.

Gross, J., Burchard, M., Schertl, H-P., and Maresch, W.V. (2008) Common high-pressure metamorphic history of eclogite lenses and surrounding metasediments: a case study of calc–silicate reaction zones (Erzgebirge, Germany). European Journal of Mineralogy, 20, 757-775.

Guo, S., Chen, Y., Liu, C-Z., Wang, J-G., Su, B., Gao, Y-J., Wu, F-Y., Sein, K., Yang, Y-H., and Mao, Q. (2016) Scheelite and coexisting F-rich zoned garnet, vesuvianite, fluorite, and apatite in calc-silicate rocks from the Mogok metamorphic belt, Myanmar: implications for metasomatism in marble and the role of halogens in W mobilization and mineralization. Journal of Asian Earth Sciences, 117, 82-106.

Hofmeister, A.M., Schaal, R.B., Campbell, K.R., Berry, S.L., and Fagan, T.J. (1998) Prevalence and origin of birefringence in 48 garnets from the pyrope—almandine—grossularite—spessartine quaternary. American Mineralogist, 83, 1293-1301.

Holten, T., Jamtveit, B., and Meakin, P. (2000) Noise and oscillatory zoning of minerals. Geochimica et Cosmochimica Acta, 64, 1893-1904.

Holten, T., Jamtveit, B., Meakin, P., Cortini, M., Blundy, J., and Austrheim, H. (1997) Statistical characteristics and origin of oscillatory zoning in crystals. American Mineralogist, 82, 596-606.

Hu, X. L., Ding, Z. J., He, M. C., Yao, S. Z., Zhu, B. P., Shen, J., Chen, B. (2014) Two epochs of magmatism and metallogeny in the Cuihongshan Fe-polymetallic deposit, Heilongjiang Province, NE China: constrains from U-Pb and Re-Os geochronology and Lu-Hf isotopes. Journal of Geochemical Exploration, 143, 116-126.

Huckenholz, H.G., Fehr, K.T. (1982) Stability relationships of grossular+quartz+wollastonite+anorthite. II. The effect of grandite-hydrograndite solid solution. Neues Jahrbuch fur Mineralogie. Abhandlungen, 145, 1-33.

Ismail, R., Ciobanu, C.L., Cook, N.J., Teale, G.S., Giles, D., Mumm, A.S., and Wade, B. (2014) Rare earths and other trace elements in minerals from skarn assemblages, Hillside iron oxide–copper–gold deposit, Yorke Peninsula, South Australia. Lithos, 184-187, 456-477.

Jaffe, H.W. (1951) The role of yttrium and other minor elements in garnet group. American Mineralogist, 36, 133-155.

Jamtveit, B. (1991) Oscillatory zonation patterns in hydrothermal grossular-andradite garnet: nonlinear dynamics in regions of immiscibility. American Mineralogist, 76, 1319-1327.

Jamtveit, B., and Hervig, R.L. (1994) Constraints on transport and kinetics in hydrothermal systems from zoned garnet crystals. Science, 263, 505-508.

Jamtveit, B., Ragnarsdottir, K.V., and Wood, B.J. (1995) On the origin of zoned grossular-andradite garnets in hydrothermal systems. European Journal of Mineralogy, 7, 1399-1410.

Jamtveit, B., Wogelius, R.A., and Fraser, D.G. (1993) Zonation patterns of skarn garnets: records of hydrothermal system evolution. Geology, 21, 113-116.

Lessing, P., and Standish, R.P. (1973) Zoned garnet from Crested Butte, Colorado. American Mineralogist, 58, 840-842.

Locock, A.J. (2008) An Excel spreadsheet to recast analyses of garnet into end-member components, and a synopsis of the crystal chemistry of natural silicate garnets. Computer & Geosciences, 34, 1769-1780.

Manning, C.E., and Bird, D.K. (1990) Fluorian garnets from the host rocks of the Skaergaard intrusion: implications for metamorphic fluid composition. American Mineralogist, 77, 859-873.

Mao, J.W., Pirajno, F., and Cook, N. (2011) Mesozoic metallogeny in East China and corresponding geodynamic settings: an introduction to the special issue. Ore Geology Reviews, 43, 1-7.

McAloon, B. P., and Hofmeister, A. M. (1993) Single-crystal absorption and reflection infrared spectroscopy of birefringent grossular-andradite garnets. American Mineralogist, 78, 957-967.

Meinert, L.D., Dipple, G.M., and Nicolescu, S. (2005) World skarn deposit. Economic Geology, 100, 299-336.

Moretti, R., and Ottonello, G. (1998) An appraisal of endmember energy and mixing properties of the rare earth garnets. Geochimica et Cosmochimica Acta, 62, 1147-1173.

Orhan, A. (2017) Evolution of the Mo-rich scheelite skarn mineralization at Kozbudaklar, Western Anatolia, Turkey: evidence from mineral chemistry and fluid inclusions. Ore Geology Reviews, 80, 141-165.

Ottonello, G., Bokreta, M., and Sciuto, P.F. (1996) Parameterization of energy and interactions in garnets: end-member properties. American Mineralogist, 81, 429-447.

Park, C., Choi, W., Kim, H., Park, M., Kang, I., and Lee, H. (2017) Oscillatory zoning in skarn garnet: implication for tungsten ore exploration. Ore Geology Reviews, 89, 1006-1018.

Park, C., Choi, W., Kim, H., Park, M. H., Kang, I. M., and Lee, H. S. (2018) Oscillatory zoning in skarn garnet: Implications for tungsten ore exploration. Ore Geology Reviews, 89, 1006-1018.

Peng, H-J., Mao, J.W., Hou, L., Shu, Q-H., Zhang, C-Q., Liu, H., and Zhou, Y-M. (2016) Stable isotope and fluid inclusion constraints on the source and evolution of ore fluids in the Hongniu-Hongshan Cu skarn deposit, Yunnan Province, China. Economic Geology, 111, 1369-1396.

Pollok, K., Jamtveit, B., and Purnis, A. (2001) Analytical transmission electron microscopy of oscillatory zoned grandite garnets. Contributions to Mineralogy and Petrology, 141, 358-366.

Ranjbar, S., Tabatabaei Manesh, S.M., Mackizadeh, M.A., Tabatabaei, S.H., and Parfenova, O.V. (2016) Geochemistry of major and rare earth elements in garnet of the Kale Kafi skarn, Anarak Area, Central Iran: constraints on processes in a hydrothermal system. Geochemistry International, 54(5), 423-438.

Rossman, G.R., and Aines, R.D. (1991) The hydrous components in garnets: grossular-hydrogrossular. American Mineralogist, 76, 1153-1164.

Sepidbar, F., Mirnejad, H., Li, J., Wei, C., and George, L.L. (2017) Mineral geochemistry of the Sangan skarn deposit, NE Iran: implication for the evolution of hydrothermal fluid. Geochemistry, 77(3), 399-419.

Shannon, R.D. (1976) Revised effective ionic radii and systematic studies of interatomic distances in halides and calcogenides. Acta Crystallographica, A32, 751-767.

Shore, M., and Fowler, A.D. (1996) Oscillatory zoning in minerals: a common phenomenon. Canadian Mineralogist, 34, 1111-1126.

Smith, M.P., Henderson, P., Jeffries, T.E.R., Long, J., and Williams, C.T. (2004) The rare earth elements and Uranium in garnets from the Beinn an Dubhaich Aureole, Skye, Scotland, UK: constraints on processes in a dynamic hydrothermal system. Journal of Petrology, 45, 457-484.

Streck, M.J. (2008) Mineral textures and zoning as evidence for open system processes. Reviews in Mineralogy & Geochemistry, 69, 595-622

Sun, S.S., and McDonough, W.F. (1989) Chemical and isotopic systematic of oceanic basalts: implications for mantle composition and processes. Geological Society, London, Special Publications, 42, 313-345.

van Westrenen, W., Allan, N.L., Blundy, J.D., Lavrentiev, M.Y., Lucas, B.R., Purton, J.A. (2003) Dopant incorporation into garnet solid solutions-a breakdown of Goldschmidt's first rule. Chemical Communications, 6, 767-787.

Wang, L.P., Essene, E.J., and Zhang, Y. (2000) Direct observation of immiscibility in pyrope-almandine-grossular garnet. American Mineralogist, 85, 41-46.

White, W.M. (2013) Geochemistry, 600 p. Wiley-Blackwell, New York.

Xie, G. Q., Mao, J. W., Bagas, L., Fu, B., and Zhang, Z. Y. (2019) Mineralogy and titanite geochronology of the Caojiaba W deposit, Xiangzhong metallogenic province, southern China: implications for a distal reduced skarn W formation. Mineralium Deposita, 54(3), 459-472

Xu, J., Ciobanu, C.L., Cook, N.J., Zheng, Y., Sun, X., and Wade, B.P. (2016) Skarn formation and trace elements in garnet and associated minerals from Zhibula copper deposit, Gangdese Belt, southern Tibet. Lithos, 262, 213-231.

Yardley, B.W.D., Rochelle, C.A., Barnicoat, A.C., and Lloyd, G.E. (1991) Oscillatory zoning in metamorphic minerals: an indicator of infiltration metasomatism. Mineralogical Magazine, 55, 357-365.

Yu, J. J., Wang, F., Xu, W. L., Gao, F. H., and Pei, F. P. (2012) Early Jurassic mafic magmatism in the Lesser Xing'an-Zhangguangcai Range, NE China, and its tectonic implications: constraints from zircon U-Pb chronology and geochemistry.

Lithos, 142-143, 256-266.

Zaw, K., and Singoyi, B. (2000) Formation of magnetite-scheelite skarn mineralization at Kara, Northwestern Tasmania: evidence from mineral chemistry and stable isotopes. Economic Geology, 95, 1215-1230.

Zhang, Y., Shao, Y., Wu, C., and Chen, H. (2017) LA-ICP-MS trace element geochemistry of garnets: constraints on hydrothermal fluid evolution and genesis of the Xinqiao Cu-S-Fe-Au deposit, eastern China. Ore Geology Reviews, 86, 426-439.

Zhao, W.W., Zhou, M-F., Chen, W.T. (2016) Growth of hydrothermal baddeleyite and zircon in different stages of skarnization. American Mineralogist, 101, 2689-2700.

Figure Captions

Figure. 1 Schematic illustration of (a) tectonic subdivisions of China (after Mao et al. 2011) and (b) sketch geological map of the eastern part of the Central Asian Orogenic Belt (modified from Fei et al. 2018).

Figure 2 (a) Schematic geological map of the Cuihongshan polymetallic deposit. (b) Cross-section map of the 44th exploration line. (c) Cross-section map of the 57th exploration line (modified from Fei et al. 2018).

Figure 3 Photomicrographs of garnet grains in the Cuihongshan deposit (b-d, g, k and p were taken with cross polarized light; j, l and o were taken with plane polarized light. Photomicrographs of e, h and m are BSE images.). (a) Type I garnets in hand specimen coexisting with clinopyroxene and cut by magnetite. (b) Type I garnet shows polysynthetic twinning. (c) Type I garnets cut by diopside. (d-e) Type I garnet showing compositional zonation polysynthetic twinning are not consistent in one grain. (f) Type II garnet in hand specimen cutting the early formed clinopyroxene. (g-h) Anisotropic type II garnet developing oscillatory zoning. (i) Type III garnet occurring as aggregates. (j-k, m) Isotropic type III garnet exhibiting zonation transition from a planar dodecahedral {110} crystal faces growth in the core to a subsequently composite dodecahedral {110}-trapezohedral {211} crystal faces growth in the margin (l) type III garnet cutting diopside and magnetite (n) Type IV garnets occurring as veins. (o-p) Euhedral garnet veins in magnesian skarn rocks were replaced by magnetite. Mineral abbreviations: Chl-chlorite; Cpx-clinopyroxene;

Fl-fluorite; Grt-garnet; Mag-magnetite; Tr-tremolite.

Figure 4 Ternary diagram summarizing garnet compositions in the Cuihongshan deposits (modified from Meinert et al. 2005). Grs-grossular; Adr-andradite; Alm+Sps+Uv+Prp-almandine+spessartine+uvarovite+pyrope.

Figure 5 X-ray element mapping of iron, aluminum, tin, fluorine, manganese and tungsten in different types of garnets from the Cuihongshan skarn deposit.

Figure 6 Variation of F content within andradite composition in garnets from the Cuihongshan deposit.

Figure 7 Chondrite-normalized rare earth element patterns for single garnet grains and different types of garnets, including type I (a-b), type II (c-d), type III (e-f) and type IV (g) garnet grains in the Cuihongshan deposit. Normalized values are from Sun and McDonough (1989).

Figure 8 (a) W versus X_{Adr} of garnets from the Cuihongshan deposit; (b) Sn versus X_{Adr} of garnets from the Cuihongshan deposit; (c) REE, LREE and HREE versus X_{Adr} of garnets from the Cuihongshan deposit; (d) REE versus X_{Adr} for different types of garnets from the Cuihongshan deposit; (e) Eu anomaly as a function X_{Adr} for different types of garnets from Cuihongshan deposit. Eu/Eu*>1 indicates a positive Eu anomaly. (f) LREE/HREE fractionation as a function of X_{Adr} for different types of garnets from the Cuihongshan deposit.

Appendix Captions

Appendix 1 Analytical methods of garnets in the Cuihongshan deposit, Lesser Xing’an Range, NE China.

Appendix 2 Composition distribution of the garnet grains in the Cuihongshan deposit.

Appendix 3 Major and trace elements compositional variations of zoned garnet in the calcic skarn rocks (Type I garnet: ECH44-5; Type II garnet: CH-11; Type III garnet: ECH44-1-5)

Appendix 4 $REE_3Al_5O_{12}$ and $REE_3Fe_5O_{12}$ hydrolysis as a function of P and T via SUPCRT92 package (modified from Gaspar et al. 2008).

Appendix 5 Enthalpy of mixing for low molar fractions (dilute range) of REE garnet components $X_{REE,\ VIII}$. All lines represent the result of static potential calculation for the mixtures of interest (Gaspar et al. 2008).

Appendix-Table Representative electron microprobe (EMPA) data of different types of garnets from the Cuihongshan deposit (calculated based on Locock 2008, see Table 1) and Representative LA-ICP-MS analyses of different types of garnets from the Cuihongshan deposit (see Table 2)

Figure 1

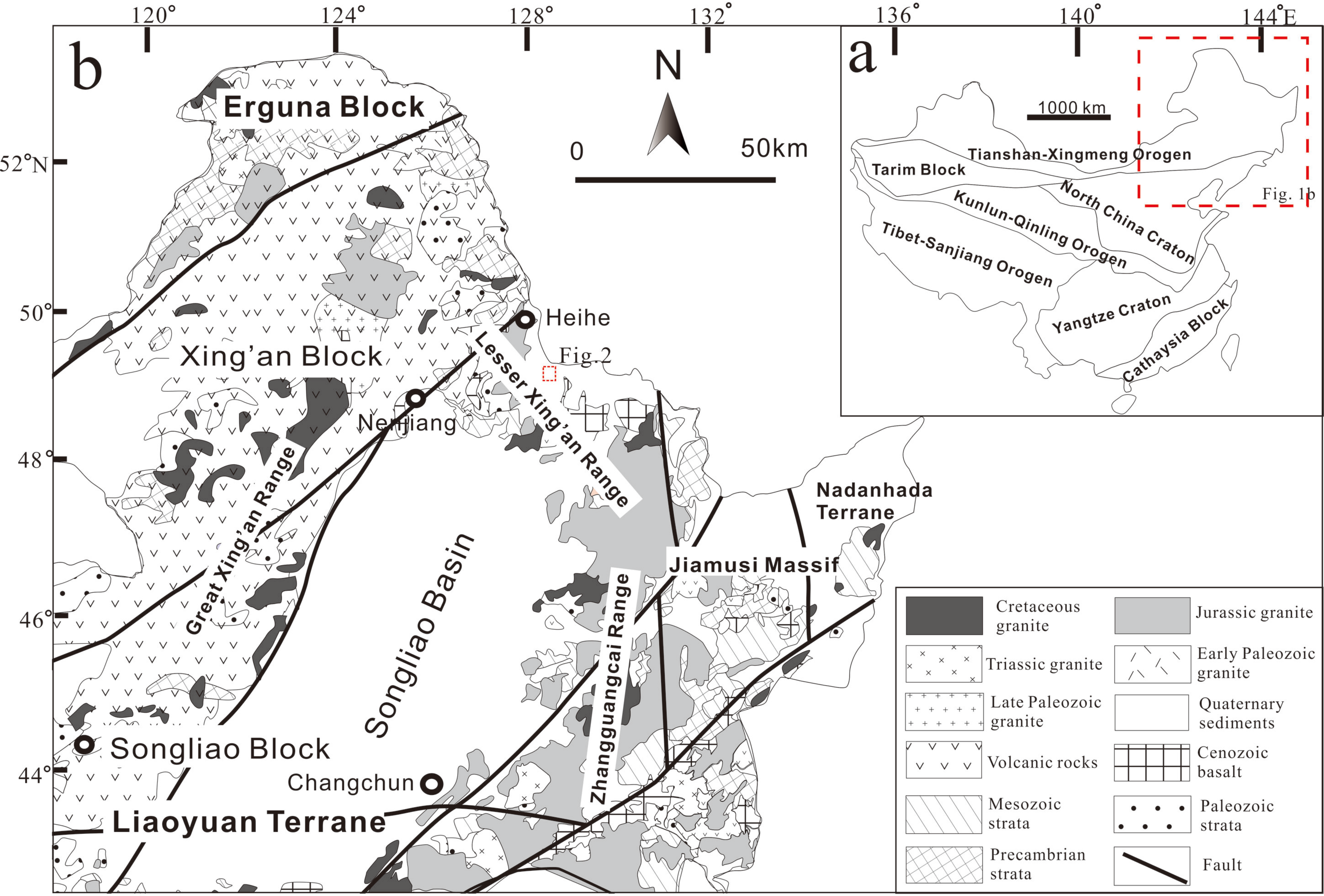

b
a
120°
124°
128°
132°
136°
140°
144°E
52°N
50°
48°
46°
44°
N
0
50km
Erguna Block
Xing'an Block
Heihe
Fig.2
Nenjiang
Lesser Xing'an Range
Great Xing'an Range
Songliao Basin
Songliao Block
Changchun
Liaoyuan Terrane
Zhangguangcai Range
Jiamusi Massif
Nadanhada Terrane
1000 km
Tianshan-Xingmeng Orogen
Tarim Block
North China Craton
Kunlun-Qinling Orogen
Tibet-Sanjiang Orogen
Yangtze Craton
Cathaysia Block
Fig. 1b
Cretaceous granite
Jurassic granite
Triassic granite
Early Paleozoic granite
Late Paleozoic granite
Quaternary sediments
Volcanic rocks
Cenozoic basalt
Mesozoic strata
Paleozoic strata
Precambrian strata
Fault

Figure2


128 44'08"E
128 45'00"E
48 29'30"N
48 28'30"N
a
No. I
No. III
No. II
Type I
Type II
Type III
Type IV
Exploration Line57th
Exploration Line 44th
A
A'
B
B'
0
200m
b
Surface=420 m
61° 20'
Quaternary Sediments
400 m
300 m
200 m
100 m
0 m
-100 m
ECH44-5,6,7,8
ECH44-1'
ECH44-4
CH-16,17
CH-22,24,25
CH-11
c
Calcic Skarn Rocks
Magnesian Skarn Rocks
Exploration Line
CHYQ-4
CHYQ-5,9
ECH58-29
ECH58-44
0
100 m
Scheelite-Molybdenite orebody
Chalcopyrite-Galena-Sphalerite orebody
Magnetite-Scheelite-Molydenite orebody
Sphalerite orebody
Magnetite orebody
Magnetite-Sphalerite orebody
Porphyritic granite
Monzogranite
Porphyritic quartz monzonite
Biotite porphyritic granite
Biotite syenogranite
Sandstone and siltstone
Limestone and dolomitic limestone
Calcic Skarn
Magnesian Skarn

Figure 3

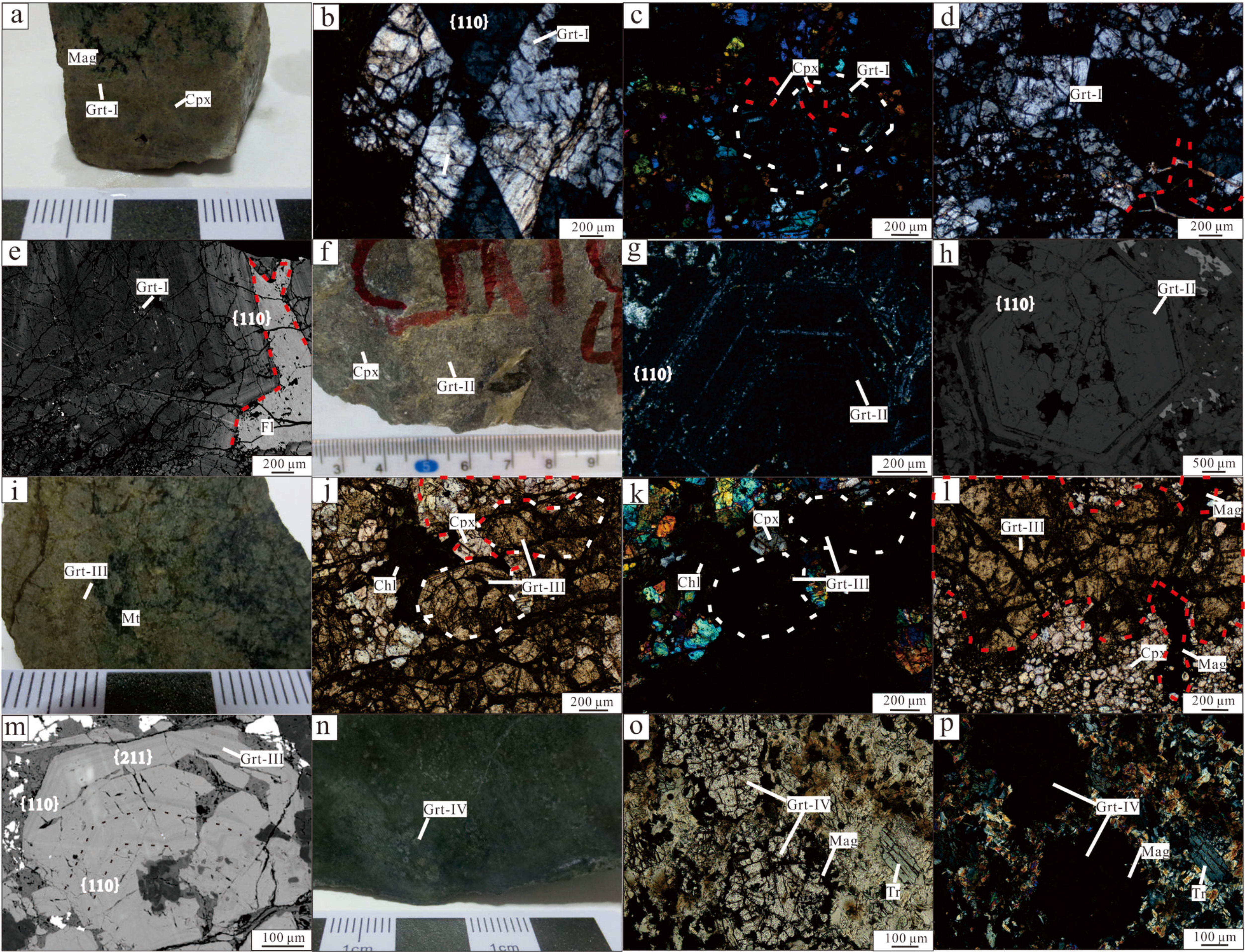
a
Mag
Grt-I
Cpx
b
{110}
Grt-I
200 μm
c
Cpx
Grt-I
200 μm
d
Grt-I
200 μm
e
Grt-I
{110}
Fl
200 μm
f
Cpx
Grt-II
3
4
5
6
7
8
9
g
{110}
Grt-II
200 μm
h
{110}
Grt-II
500 μm
i
Grt-III
Mt
j
Cpx
Chl
Grt-III
200 μm
k
Cpx
Chl
Grt-III
200 μm
l
Grt-III
Mag
Cpx
Mag
200 μm
m
{211}
Grt-III
{110}
{110}
100 μm
n
Grt-IV
1cm
1cm
o
Grt-IV
Mag
Tr
100 μm
p
Grt-IV
Mag
Tr
100 μm

Figure 4

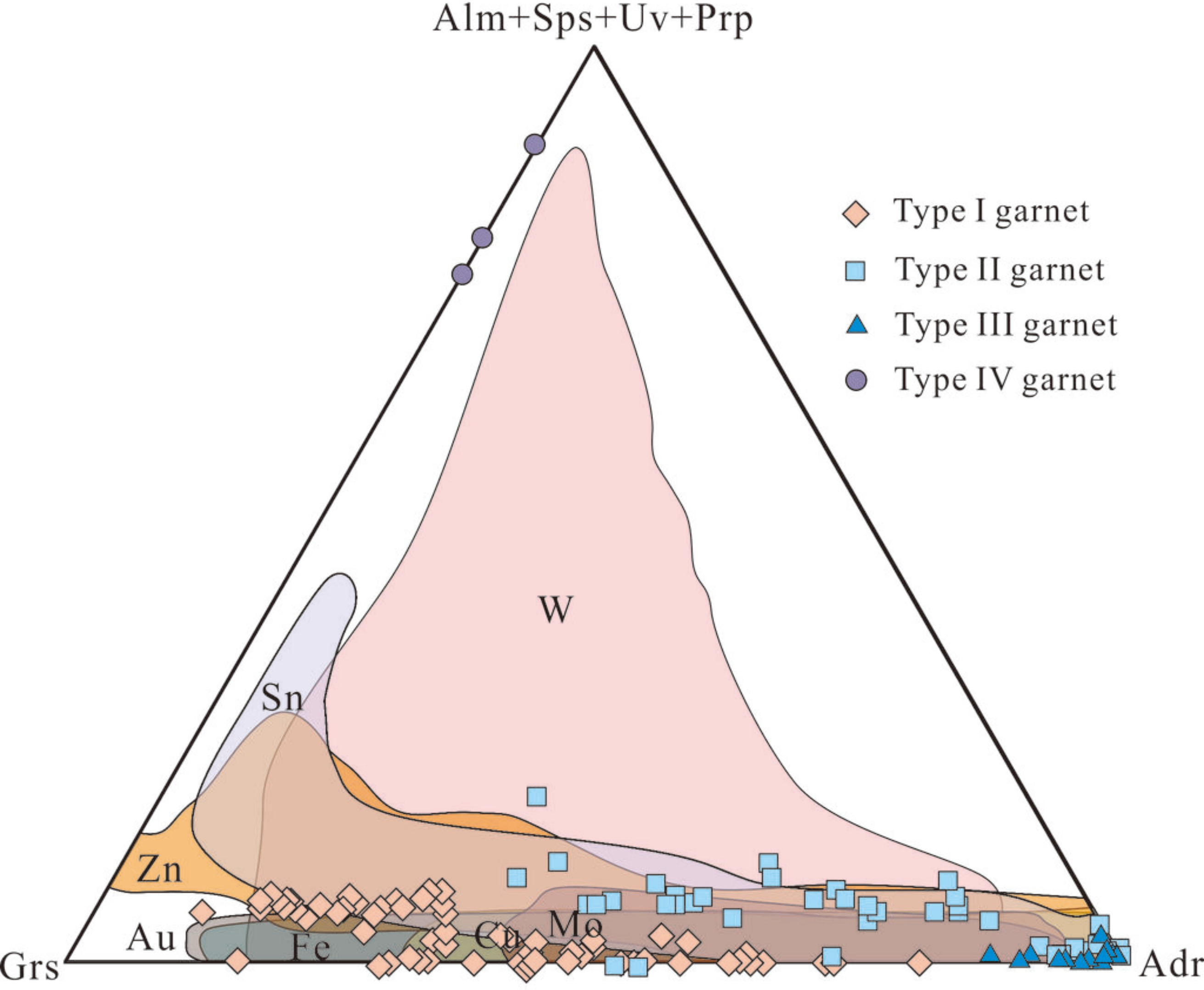
Alm+Sps+Uv+Prp
Grs
Adr
W
Sn
Zn
Au
Fe
Cu
Mo
Type I garnet
Type II garnet
Type III garnet
Type IV garnet

Figure 5

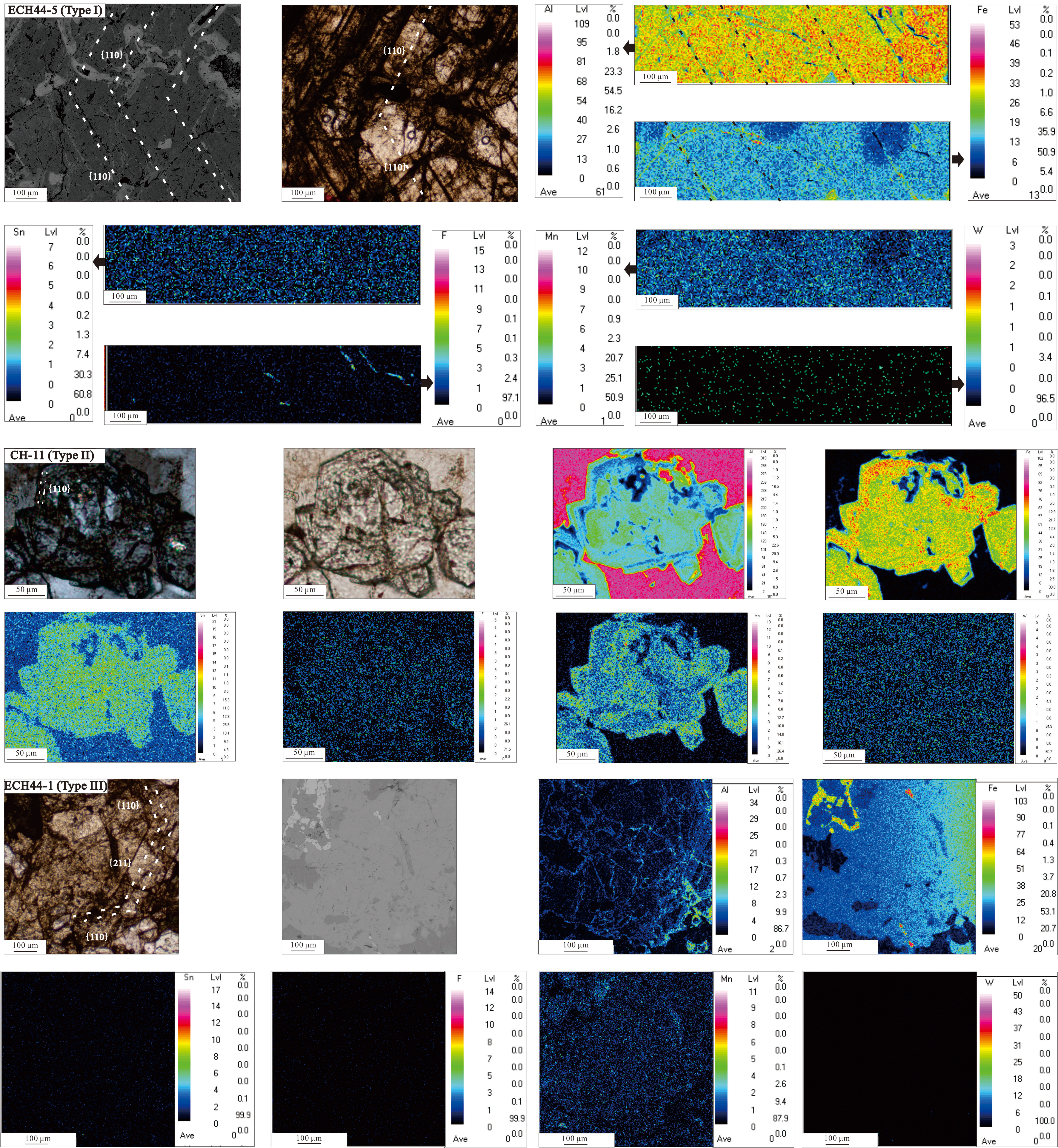
ECH44-5 (Type I)
{110}
{110}
100 µm
{110}
{110}
100 µm
Al Lvl %
109 0.0
95 0.0
81 1.8
68 23.3
54 54.5
40 16.2
27 2.6
13 1.0
0 0.6
Ave 61 0.0
100 µm
100 µm
Fe Lvl %
53 0.0
46 0.0
39 0.1
33 0.2
26 1.0
19 6.6
13 35.9
6 50.9
0 5.4
Ave 13 0.0
Sn Lvl %
7 0.0
6 0.0
5 0.0
4 0.0
3 0.2
2 1.3
1 7.4
0 30.3
0 60.8
Ave 0 0.0
100 µm
100 µm
F Lvl %
15 0.0
13 0.0
11 0.0
9 0.0
7 0.1
5 0.1
3 0.3
1 2.4
0 97.1
Ave 0 0.0
Mn Lvl %
12 0.0
10 0.0
9 0.0
7 0.0
6 0.9
4 2.3
3 20.7
1 25.1
0 50.9
Ave 1 0.0
100 µm
100 µm
W Lvl %
3 0.0
2 0.0
2 0.0
1 0.1
1 0.0
0 0.0
0 3.4
0 0.0
0 96.5
Ave 0 0.0
CH-11 (Type II)
{110}
50 µm
50 µm
50 µm
50 µm
50 µm
50 µm
50 µm
50 µm
ECH44-1 (Type III)
{110}
{211}
{110}
100 µm
100 µm
Al Lvl %
34 0.0
29 0.0
25 0.0
21 0.0
17 0.3
12 0.7
8 2.3
4 9.9
0 86.7
Ave 2 0.0
100 µm
Fe Lvl %
103 0.0
90 0.0
77 0.1
64 0.4
51 1.3
38 3.7
25 20.8
12 53.1
0 20.7
Ave 20 0.0
100 µm
Sn Lvl %
17 0.0
14 0.0
12 0.0
10 0.0
8 0.0
6 0.0
4 0.0
2 0.1
0 99.9
Ave 0 0.0
100 µm
F Lvl %
14 0.0
12 0.0
10 0.0
8 0.0
7 0.0
5 0.0
3 0.0
1 0.1
0 99.9
Ave 0 0.0
100 µm
Mn Lvl %
11 0.0
9 0.0
8 0.0
6 0.0
5 0.0
4 0.1
2 2.6
1 9.4
0 87.9
Ave 0 0.0
100 µm
W Lvl %
50 0.0
43 0.0
37 0.0
31 0.0
25 0.0
18 0.0
12 0.0
6 0.0
0 100.0
Ave 0 0.0
100 µm

Figure 6

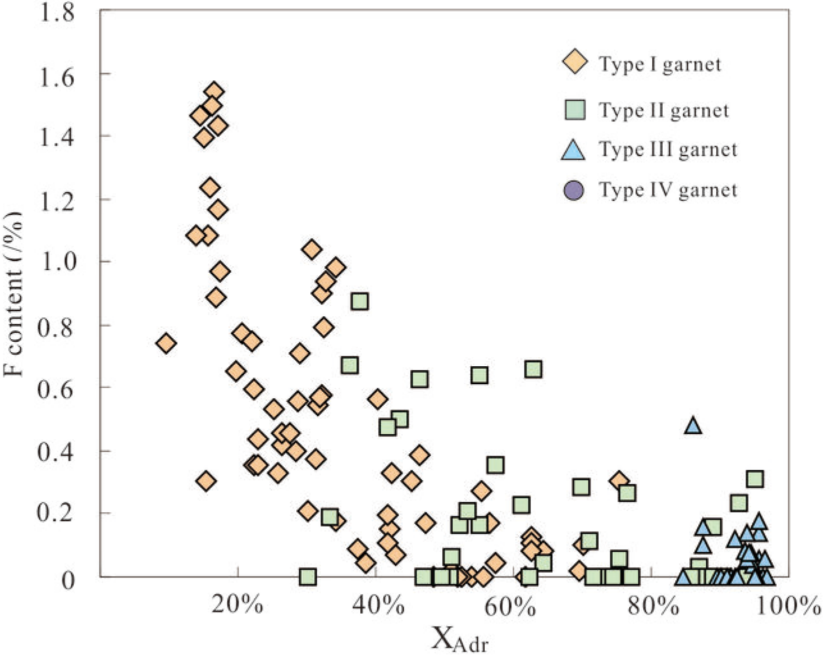
F content (/%)
1.8
1.6
1.4
1.2
1.0
0.8
0.6
0.4
0.2
0
20%
40%
60%
80%
100%
X_{Adr}
Type I garnet
Type II garnet
Type III garnet
Type IV garnet

Figure 7

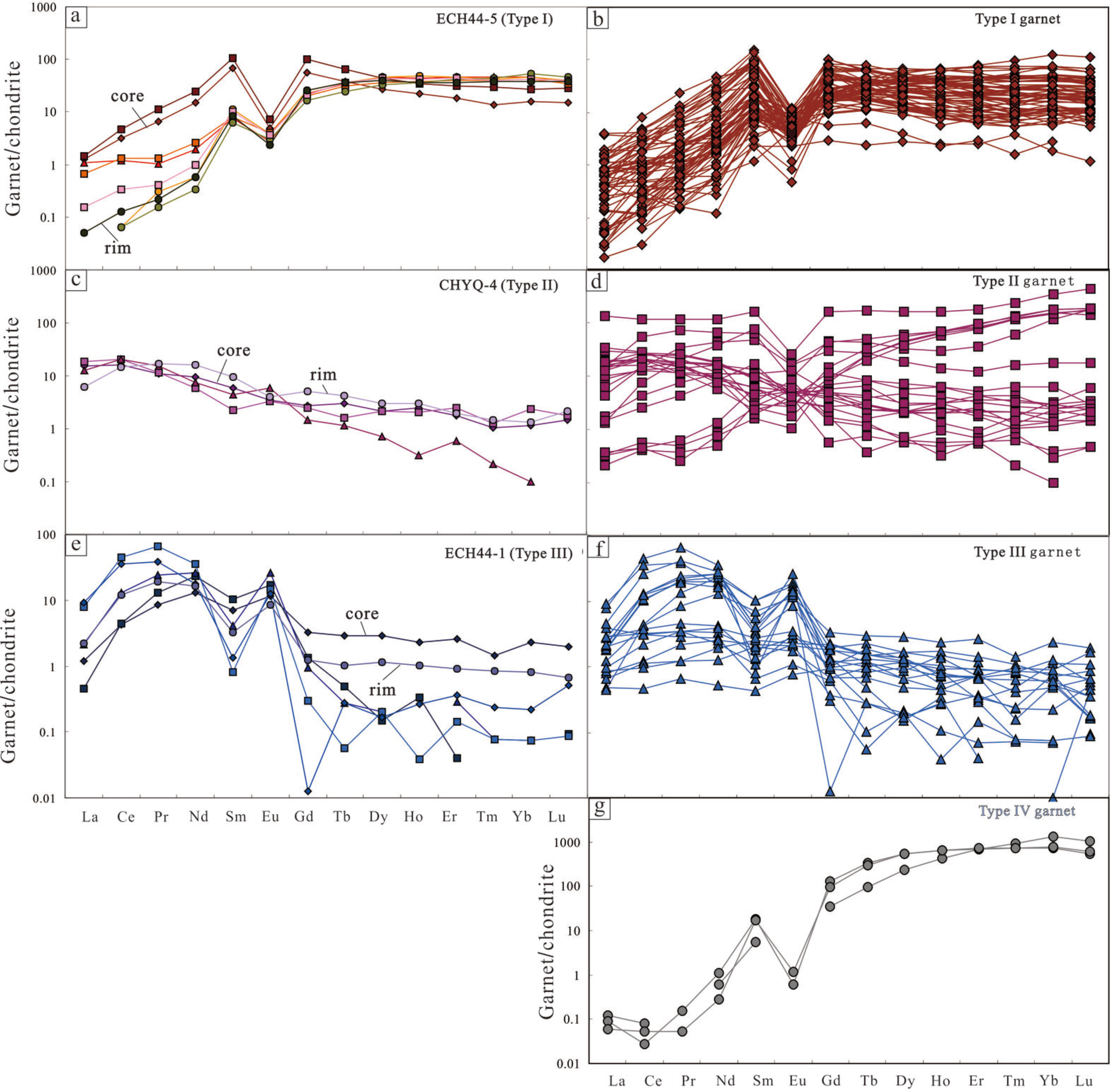
a
ECH44-5 (Type I)
core
rim
b
Type I garnet
c
CHYQ-4 (Type II)
core
rim
d
Type II garnet
e
ECH44-1 (Type III)
core
rim
f
Type III garnet
g
Type IV garnet
Garnet/chondrite
1000
100
10
1
0.1
0.01
La
Ce
Pr
Nd
Sm
Eu
Gd
Tb
Dy
Ho
Er
Tm
Yb
Lu

Figure 8

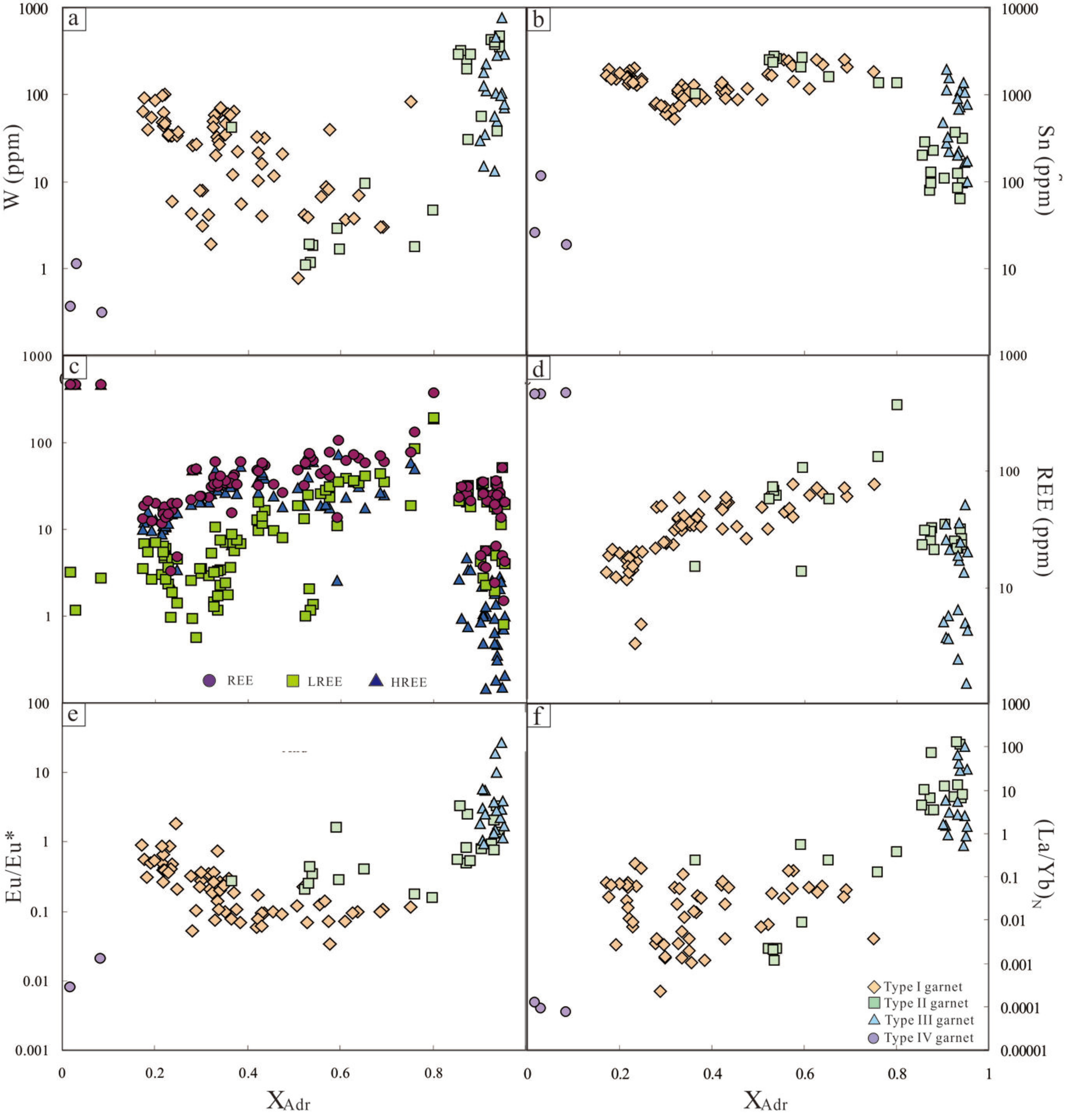
a
b
c
d
e
f
W (ppm)
Sn (ppm)
REE (ppm)
Eu/Eu*
(La/Yb)$_N$
1000
100
10
1
10000
1000
100
10
1000
100
10
1
1000
100
10
100
10
1
0.1
0.01
0.001
1000
100
10
1
0.1
0.01
0.001
0.0001
0.00001
0
0.2
0.4
0.6
0.8
1
X$_{Adr}$
X$_{Adr}$
REE
LREE
HREE
Type I garnet
Type II garnet
Type III garnet
Type IV garnet